We are IntechOpen, the world's leading publisher of Open Access books Built by scientists, for scientists

4,800
Open access books available

122,000
International authors and editors

135M
Downloads

Our authors are among the

154
Countries delivered to

TOP 1%
most cited scientists

12.2%
Contributors from top 500 universities

CLARIVATE ANALYTICS BOOK CITATION INDEX INDEXED

WEB OF SCIENCE™

Selection of our books indexed in the Book Citation Index in Web of Science™ Core Collection (BKCI)

Interested in publishing with us?
Contact book.department@intechopen.com

Numbers displayed above are based on latest data collected.
For more information visit www.intechopen.com

Chapter 2

Recent Computer-Aided Design Techniques for Rectangular Microstrip Antenna

Sudipta Chattopadhyay and

Subhradeep Chakraborty

Additional information is available at the end of the chapter

http://dx.doi.org/10.5772/66355

Abstract

In modern microwave systems, rectangular microstrip patch antennas (RMPAs) are probably the most investigated topics among the planar antennas. There are several methods available in literature, for designing and analyzing such antennas, but most of them are very complex and give only approximate results. In this chapter, we have discussed the most accurate and updated computer-aided design (CAD) formulations related to probe-fed RMPA for computing its fundamental input characteristics (resonant frequency and input impedance) and improving radiation characteristics, i.e. gain and polarization purity (the parameter that signifies how much an RMPA is free from spurious modes). These formulations have evolved in the last decades and have been validated against numerous simulations and measurements. The present CAD formulas for resonant frequency and input impedance can accurately address a wide range of RMPA with patch width to patch length ratio (W/L) from 0.5 to 2.0, a substrate having thickness up to 0.23 λ_g where λ_g is the guide wavelength and relative permittivity (ε_r) ranging over 2.2–10.8. The role of a finite air gap on resonant frequency and gain of an RMPA have also been presented. The chapter will be surely useful to antenna designers to achieve a concrete understanding of the RMPA theory.

Keywords: rectangular microstrip antenna, resonant frequency, input impedance, gain, polarization purity, grounded microstrip patch

1. Introduction

'Microstrip antennas', the class of antennas which has been capturing the attention of the antenna research community for the last 63 years, starting from the 3rd Symposium on the US Air Force Antenna Research and Development Program, was proposed firstly by Deschamp and Sichak [1] in 1953. In [1], they proposed a microstrip feeding network for a waveguide system which comprised of 300 waveguide horn antennas. But, the 'microstrip patch', to which all the researchers associated to the antenna theory are familiar with, was theoretically analyzed by Howell in [2] and applied into practical applications by Munson in [3] for the first time. Still, the credit of the authors of the work [1] was to foster a very much new discipline of antenna engineering, and in addition to this, they highlighted the related performance superiority of this new antenna over the other commercially available conventional antenna. From 1972 onwards, researchers started to understand a microstrip patch in two approaches: (i) treating the patch as a lossy and open resonator cavity [2] and (ii) as an extended section of a microstrip line [3].

In the last four decades, several books [4–11] and collection of research papers [12, 13] have been published unfolding rigorous analytical and numerical techniques dealing with microstrip antennas. The computational methods like FDTD, FEM and MOM are very much versatile in nature particularly in analyzing irregular-shaped patch geometries with huge various types of substrates, but any of them give neither any physical insights into the radiation mechanism of the antenna nor any closed-form design formulations which are utmost necessary to any practicing antenna engineer, researcher, academician or scientist. In this context, cavity resonator model appears to be more effective than the other available methods to estimate the fundamental input characteristics (i.e. resonant frequency and input impedance) and to improve the crucial radiation characteristics (i.e. gain and polarization purity) for commonly available microstrip antennas of regular geometries with thin substrate. This method not only improvises the design steps of antenna design but also aids in achieving better performance.

In this chapter, the authors have presented comprehensive electromagnetic analyses on the fundamental input characteristics (i.e. resonant frequency and input impedance) and radiation characteristics (i.e. gain and polarization purity) of rectangular microstrip antennas with conventional and suspended geometries in light of the versatile cavity model method and discussed some improved and closed-form computer-aided design (CAD) formulas. Unlike other theories and work, the present CAD formulas can accurately address a wide range of aspect ratio or patch width to patch length ratio (W/L) from 0.5 to 2.0, a substrate having thickness up to 0.23 λ_g where λ_g is the guide wavelength and relative permittivity (ε_r) ranging over 2.2–10.8. (Discuss Novelty) A coaxially fed RMPA with length L and width W on a substrate (ε_r) above a variable air-gap over the ground plane is shown in **Figure 1**.

Air gap over the ground plane is shown in **Figure 1**. The variable air-gap height h_1 can be decreased to zero to achieve the conventional form. The fringing of the electric fields at the radiating and non-radiating edges of the rectangular patch is taken into account in terms of ΔL and ΔW, respectively. The present CAD formulas were introduced firstly in [14] by Chattopadhyay et al.

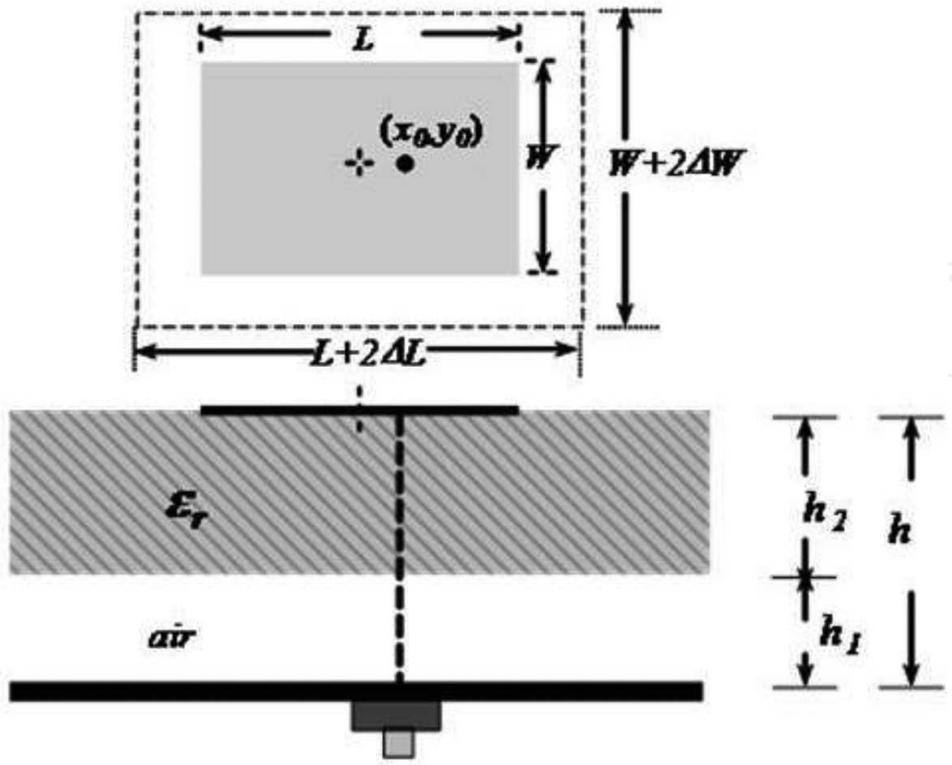

Figure 1. Schematic diagram of a coax-fed rectangular microstrip patch antenna (RMPA).

2. Input characteristics

2.1. Resonant frequency

After the work of Howell [2], Hammerstad [15] proposed comprehensive CAD formulations on resonance characteristics of an RMPA using the cavity resonator model (CRM) method. Till now, several theoretical analyses employing CRM method [6, 16–18], transmission-line method [19, 20], method of moments [21, 22] and integral equation technique [23] are available in literature. But the CAD formulas presented in [6, 15] are found to be the most popular for the design purpose.

Nevertheless, a close inspections into these works show that the formulas available in [6, 15] can provide a reasonably good approximation only when the patches have aspect ratio (W/L) near to 1.5 and the substrate thickness is lower than 0.02 λ_g, where λ_g is the guide wavelength at the resonant frequency f_r. Also, the computed f_r values using formulas in [6, 15] show errors in comparison with the measurements which can be found in [24, 25]. Those works [24, 25] used around 0.04 λ_g to 0.23 λ_g substrate thickness. The use of an air gap in between the substrate and the ground plane has been found in [26–34] which helps in achieving tunability of an RMPA and enhancing its impedance bandwidth. Earlier, a cavity model was also discussed in detail in [5, 11]. In this section, authors have emphasized on a better CAD formulation as found in an earlier work of one of the present authors in [14] using the well-known CRM method called quasi-static approach [11] to estimate more accurately the dominant and the higher-order resonances in an RMPA with and without air gap. Here, ΔL and ΔW

have been considered as a function of the aspect ratio. In [14] Chattopadhyay et al. considered an equivalent circular patch with radius a, effective radius a_{eff} and same resonant frequency as that of the RMPA. This helps to establish a relationship among the fringing parameters ΔL, ΔW and a_{eff} by equating the zero-order resonant frequencies of both patches as found in one of the earlier works of Chattopadhyay in [14, 35].

From [35–38] we can write

$$f_{0,r} = \frac{c}{2L\sqrt{\varepsilon_r}} \tag{2.1}$$

where c is the velocity of light in free space. Following the earlier work of Chattopadhyay in [14, 35], we can assume that both antennas of same resonant frequencies have same circumference. Therefore, we can write

$$(\mathrm{W} + \mathrm{L}) = \pi \mathrm{a} \tag{2.2}$$

$$(\mathrm{L} + 2\Delta\mathrm{L}) + (\mathrm{W} + 2\Delta\mathrm{W}) = \pi a_{eff} \tag{2.3}$$

In Eq. (2.3) α is the first zero of the derivative of the Bessel function of order $n = 1$. Now, a_{eff} is the effective radius of a circular patch due to fringing electric fields as found in [27]:

$$a_{eff} = a\sqrt{1+q} \tag{2.4}$$

where q is the fringing factor calculated from [27] as

$$q = u + v + uv \tag{2.5}$$

and

$$u = \left(1 + \varepsilon_{re}^{-1}\right)\frac{4}{\pi a/h} \tag{2.6}$$

$$v = \frac{2}{3t} \times \frac{\ln(p)}{(8 + \pi a/h)} + \frac{(1/t - 1)}{(4 + 2.6a/h + 2.9h/a)} \tag{2.7}$$

$$t = 0.37 + 0.63\varepsilon_{re} \tag{2.8}$$

$$p = \frac{1 + 0.8\left(\frac{a}{h}\right)^2 + \left(\frac{0.31a}{h}\right)^4}{1 + 0.9\frac{a}{h}} \tag{2.9}$$

u, v, t and p all are dummy variables.

$$\varepsilon_{re} = \frac{\varepsilon_r\left(1 + \frac{h_1}{h_2}\right)}{(1 + \varepsilon_r h_1/h_2)} \tag{2.10}$$

where ε_{re} is the equivalent permittivity of the two-layer dielectric medium (**Figure 1**) having a total thickness $h = (h_1 + h_2)$.

Solving (2.1)–(2.4) and from one of the previous works of Chattopadhyay in [14, 35], one can write the following relations:

$$L = 1.7a \tag{2.11}$$

$$W = 1.44a \tag{2.12}$$

$$\Delta L + \Delta W = \frac{\pi a\sqrt{1+q} - 1}{2} \tag{2.13}$$

An empirical relation is used to determine ΔW in terms of ΔL for a wide range of W/L values, $2 > W/L > 0.5$ as

$$\Delta W = \Delta L\left(1.5 - \frac{W}{2L}\right) \tag{2.14}$$

and ΔL can be written as given in one of the previous works of Chattopadhyay in [14, 35]

$$\Delta L = \frac{\pi a\left[\sqrt{1+q} - 1\right]}{2\left[2.5 - 0.5\left(\frac{W}{L}\right)\right]} \tag{2.15}$$

Now, using the above Eqs. (2.1)–(2.15) discussed above and as in the previous work of Chattopadhyay in [14, 35], the resonant frequency of an RMPA with a variable air-gap h_1 is found as

$$f_{r,nm} = \frac{c}{2\sqrt{\varepsilon_{r,eff}}}\left[\left(\frac{n}{L+2\Delta L}\right)^2 + \left(\frac{m}{W+2\Delta W}\right)^2\right]^{1/2} \tag{2.16}$$

where $\varepsilon_{r,eff}$ is the effective relative permittivity of the medium below the patch [14, 27, 35].

$$\varepsilon_{\mathrm{r,eff}} = \frac{4\ \varepsilon_{\mathrm{re}}\ \varepsilon_{\mathrm{r,dyn}}}{\left(\sqrt{\varepsilon_{\mathrm{re}}} + \sqrt{\varepsilon_{\mathrm{r,dyn}}}\right)^2} \tag{2.17}$$

From Eq. (2.16) we can found the dominant mode of an RMPA is TM_{10}. ε_{re} is calculated using (2.10), and $\varepsilon_{r,dyn}$ is the dynamic dielectric constant as defined in [17, 28] and can be written as

$$\varepsilon_{r,dyn} = \frac{C_{dyn}\left(\varepsilon = \varepsilon_0\varepsilon_{re}\right)}{C_{dyn}\left(\varepsilon = \varepsilon_0\right)} \tag{2.18}$$

$$C_{dyn} = C_{0,dyn} + C_{e,dyn} \tag{2.19}$$

where C_{dyn} is the total dynamic capacitance of the RMPA and suffixes *0* and *e* denote the main and fringing components, respectively. $C_{0,dyn}$ and $C_{e,dyn}$ are determined as discussed in one of the previous works of the present authors in [14, 35]:

$$C_{0,dyn} = \gamma_n C_{0,stat} \tag{2.20}$$

$$C_{e,dyn} = \frac{1}{\delta} C_{e,stat} \tag{2.21}$$

The values γ_n and δ are as follows:

$$\gamma_n = 1.0 \text{ for } n = 0 \tag{2.22}$$
$$= 0.3525 \text{ for } n = 1$$
$$= 0.2865 \text{ for } n = 2$$
$$= 0.2450 \text{ for } n = 3$$

$$\delta = 1.0 \text{ for } n = 0 \tag{2.23}$$
$$= 2.0 \text{ for } n \neq 0$$

where $C_{0,stat}$ and $C_{e,stat}$ are the static main and static fringing capacitances of the disc, and these are [35]

$$C_{0,stat} = \varepsilon_0 \varepsilon_{re} \frac{\pi a^2}{h} \tag{2.24}$$

$$C_{e,stat} = C_{0,stat} q \tag{2.25}$$

Figure 2 shows the computed as obtained from the previous work of Chattopadhyay in [14, 35] and measured [24] resonant frequencies of an RMPA as a function of substrate thickness h_2. The three measured values for thin and thick substrates show close agreement with proposed formulations.

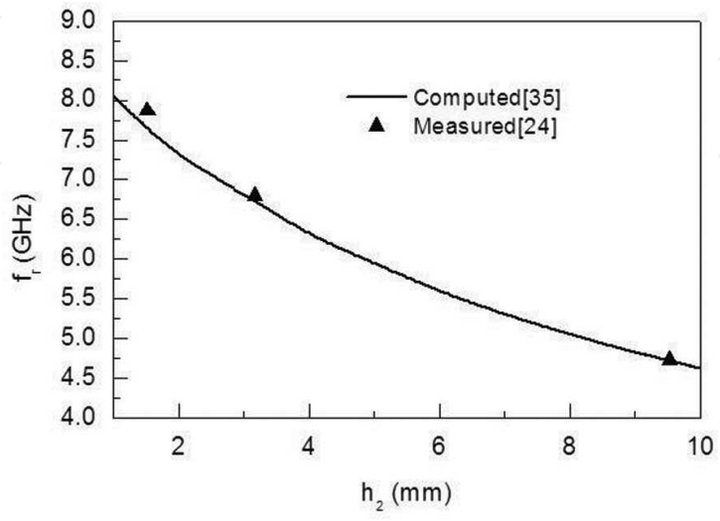

Figure 2. Resonant frequency of the dominant mode as function of substrate thickness of the RMPA, $\varepsilon_r = 2.33$, $L = 11$ mm, $W = 17$ mm, $W/L = 1.54$ [35].

In [14], Chattopadhyay et al. have also shown the close agreement between the values obtained using MOM and their theory.

Figures 3 and **4** show the computed (from the previous work of Chattopadhyay in [14, 35]), simulated and measured resonant frequencies of an RMPA with *W/L* = 1.5 having variable air-gap heights.

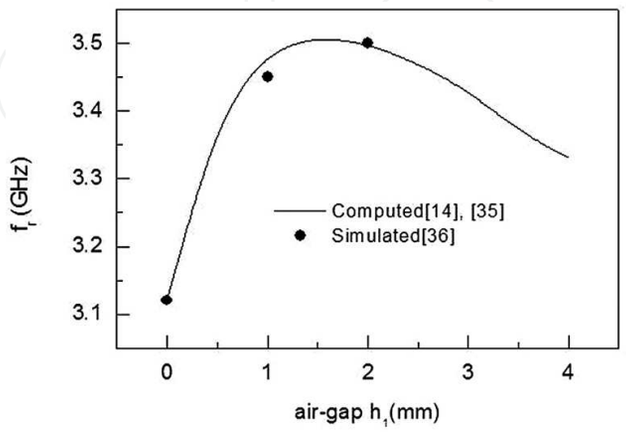

Figure 3. Resonant frequency of RMPA versus air-gap height. ε_r = 2.2, L = 30 mm, W = 45 mm, W/L = 1.5, substrate thickness h_2 = 1.575 mm [35].

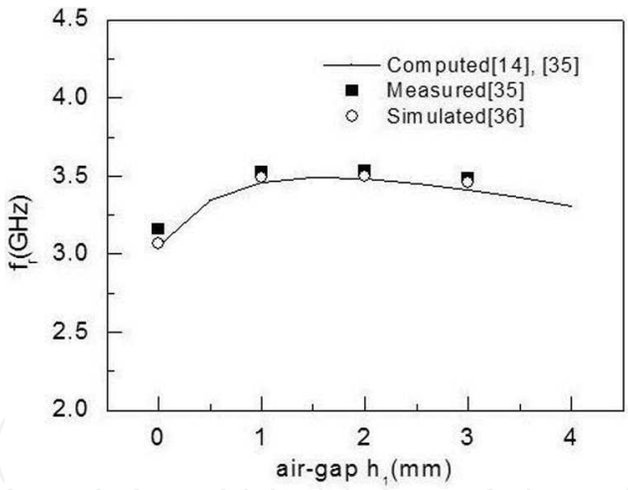

Figure 4. Dominant mode resonant frequency of RMPA versus air-gap height. ε_r = 2.33, L = 30 mm, W = 45 mm, h_2 = 1.575 mm [35].

The simulated and measured values ranging from no air gap to an air gap of 4 mm show good agreement with the present formulations. The tunability of the RMPA as a function of the air gap height has also been studied. **Table 1** compares the resonant frequencies as computed using the presented formulations (as given in the previous work of Chattopadhyay in [14, 35]) with that of Hammerstad [15], James et al. [6] and Chew and Liu [23] for different sets of RMPAs with *W/L* ≈ 1.5 and for electrical thickness ranging from 0.037 to 0.166 λ_g. The presented formulations show very close agreement with measured data [24] with an average percentage error of (1.39%) for the present formulations.

Length, L (mm)	W/L	Normalized thickness (h_2/λ_d)	Measured fr (GHz) [24]	Computed fr (GHz) [15]	Computed fr (GHz) [6]	Computed fr (GHz) [23]	Computed fr (GHz) (from the earlier work of one of the present authors in [14, 35])
38	1.5	0.037	2.31	2.38 (3.03%)	2.30 (0.4%)	2.37 (2.6%)	2.32 (0.4%)
30.5	1.49	0.047	2.89	2.90 (0.3%)	2.79 (3.4%)	2.90 (0.3%)	2.83 (2%)
19.5	1.51	0.068	4.24	4.34 (2.35%)	4.11 (3.06%)	4.32 (1.88%)	4.18 (1.4%)
13	1.5	0.094	5.84	6.12 (4.79%)	5.70 (2.39%)	6.07 (3.93%)	5.86 (0.3%)
11	1.54	0.110	6.80	7.01 (3.08%)	6.47 (4.85%)	6.90 (1.5%)	6.65 (2.2%)
9	1.55	0.125	7.70	8.19 (6.36%)	7.46 (3.11%)	7.87 (2.2%)	7.73 (0.38%)
8	1.50	0.141	8.27	9.01 (8.94%)	8.13 (1.7%)	8.39 (1.45%)	8.50 (2.7%)
7	1.50	0.148	9.14	9.97 (9.01%)	8.89 (2.73%)	8.69 (4.92%)	9.3 (1.75%)
6	1.50	0.166	10.25	11.18 (9.07%)	9.82 (4.19%)		10.4 (1.46%)
Average error w.r.t measurement [24]				**5.21%**	**2.87%**	**2.34%**	**1.39%**

Parameters: ε_r = 2.33, h_2 = 3.175 mm, for W/L = 1.5. Note: here, $\lambda_d = \lambda_g = \lambda_0/\sqrt{\varepsilon_r}$ and λ_0 are wavelengths corresponding to measured frequency.

Table 1. Comparison of the measured [24] and computed dominant mode resonant frequency of an RMPA.

Moreover, in [14] Chattopadhyay et al. showed the versatility of these formulations in accurately predicting the higher-order modes of an RMPA for W/L = 1. In [35], Chattopadhyay has predicted the higher-order modes of an RMPA for W/L = 0.7, 1.2, 1.5, 1.7 extending the work in [14]. One can refer to **Table 1** of one of the previous works of Chattopadhyay et al. in [14] for a closer look into the topic. It is seen that the significant higher-order modes of an RMPA are TM_{01}, TM_{02}, TM_{12}, TM_{20}, TM_{30}, TM_{03}, etc. When W/L = 1, TM_{10} and TM_{01} become degenerate modes. The separation between resonant frequency of dominant TM_{10} mode and that of net higher-order mode TM_{02} is from 2 to $1.25f_{r,10}$ for $0.7 < W/L < 2$ as discussed in [35] by Chattopadhyay. The effect of TM_{02} mode on the radiation characteristics of an RMPA is very detrimental [11, 14, 35], and the two newest techniques for mitigating this issue are discussed later in this chapter (see Section 4.2).

2.2. Input impedance

An RMPA can be represented as an equivalent R-L-C parallel resonant circuit in order to find out its input impedance [11]. Near resonance of the dominant mode and its input impedance can be expressed as [39, 40]

$$Z_{in}(f,x_0)=\frac{R_r}{1+Q_T^2\left(\overline{f}-\overline{f}^{-1}\right)^2}+j\left[X_f-\frac{R_rQ_T\left(\overline{f}-\overline{f}^{-1}\right)}{1+Q_T^2\left(\overline{f}-\overline{f}^{-1}\right)^2}\right] \tag{2.26}$$

where $\overline{f}=f/f_r$, f_r is the dominant mode resonant frequency and R_r is the input resistance at resonance as [8].

R_r can be expressed as

$$R_r=\frac{4h}{\pi\lambda_0}\mu\eta_0Q_T\left(\frac{L+2\Delta L}{W+2\Delta W}\right)cos^2\left(\frac{\pi(0.5L-x_0)}{L+2\Delta L}\right) \tag{2.27}$$

where η_0 is the intrinsic impedance of free space where η_0 = 377 Ω, x_0 is the distance from the centre of the patch and Q_T is the total quality factor.

Q_T can be expressed in terms of the losses due to radiation (Q_r), dielectric (Q_d) and conductor (Q_c) present in the radiating structure as given in an earlier work of one of the present authors in [40]:

$$Q_T=\left[\frac{1}{Q_r}+\frac{1}{Q_d}+\frac{1}{Q_c}\right]^{-1} \tag{2.28}$$

In this context, another parameter $\varepsilon_{r,n}$ is required to calculate Q_r and Q_d as found in [39]:

$$\varepsilon_{r,n}=\frac{\varepsilon_{reff}+1}{2} \tag{2.29}$$

Now, Q_r, Q_d and Q_c can be expressed as given in [36, 39], and an earlier work of one of the present authors in [40]:

$$Q_r=\frac{\pi}{4G_rZ_r} \tag{2.30}$$

$$Q_d=\frac{\pi(\varepsilon_r-1)\sqrt{\varepsilon_{r,n}}}{27.3(\varepsilon_{r,n}-1)\sqrt{2\varepsilon_{r,n}-1}}\frac{1}{tan\delta} \tag{2.31}$$

$$Q_c=h\sqrt{\pi f\mu_0\sigma} \tag{2.32}$$

where

$$G_r=\frac{W^2}{90\lambda_0^2}\ \text{for}\ W\le 0.35\lambda_0 \tag{2.33}$$

$$=\frac{W}{120\lambda_0}-\frac{1}{60\pi^2}\ \text{for}\ 0.35\lambda_0\le W\le 2\lambda_0$$

$$=\frac{W}{120\lambda_0}\ \text{for}\ 2\lambda_0<W$$

and

$$Z_r = \frac{120\pi\left[\frac{W}{h} + 1.393 + 0.667\ln\left(\frac{W}{h} + 1.444\right)\right]^{-1}}{\sqrt{\varepsilon_{r,n}}} \tag{2.34}$$

The same approach is also valid for circular patches, and a detailed discussion on the resonant frequency and input impedance of a circular patch can be found in [11]. From [11], one can find that the dominant mode of a circular patch is TM_{11}. The immediate higher-order modes are TM_{21}, TM_{01}, TM_{31}, etc. The formulas are found to be very accurate in case of substrate with thin and moderate height.

Cavity model analysis of the resonant frequency and input impedance for a 60°–60°–60° equilateral triangular patch is found in [5]. The dominant mode of a triangular patch is TM_{10} [5]. The immediate higher-order modes are TM_{11}, TM_{20}, TM_{21}, etc.

3. Examples

(a)Find out the resonant frequency of an RMPA with length (L) 18.2 mm and width (W) 28 mm, etched on a PTFE substrate of height 1.575 mm with dielectric constant 2.33.

(b)Repeat the problem when 1 mm air gap is introduced between substrate and ground plane.

Solution:

(a) The resonant frequency of the patch can be obtained from Eq. (3.1) as

$$f_{r,nm} = \frac{c}{2\sqrt{\varepsilon_{r,eff}}}\left[\left(\frac{n}{L + 2\Delta L}\right)^2 + \left(\frac{m}{W + 2\Delta W}\right)^2\right]^{1/2} \tag{3.1}$$

As the dominant mode is TM_{10}, $n = 1$ and $m = 0$, and therefore the Eq. (3.1) reduces to

$$f_{r,10} = \frac{c}{2\sqrt{\varepsilon_{r,eff}}}\frac{1}{L + 2\Delta L} \tag{3.2}$$

The expression for effective relative permittivity of the medium below the patch is

$$\varepsilon_{r,eff} = \frac{4\varepsilon_{re}\varepsilon_{r,dyn}}{\left(\sqrt{\varepsilon_{re}} + \sqrt{\varepsilon_{r,dyn}}\right)^2} \tag{3.3}$$

and

$$\varepsilon_{re} = \frac{\varepsilon_r\left(1 + \frac{h_1}{h_2}\right)}{(1 + \varepsilon_r h_1/h_2)} \tag{3.4}$$

As air gap height $h_2 = 0$

$$\varepsilon_{re} = \varepsilon_r = 2.33 \tag{3.5}$$

Fringing factor q is

$$q = u + v + uv \tag{3.6}$$

where

$$u = \left(1 + \varepsilon_{re}^{-1}\right)\frac{4}{\frac{\pi a}{h}} = 0.147 \tag{3.7}$$

$$t = 0.37 + 0.63\varepsilon_{re} = 1.83 \tag{3.8}$$

and

$$p = \frac{1 + 0.8\left(\frac{a}{h}\right)^2 + \left(\frac{0.31a}{h}\right)^4}{1 + 0.9\frac{a}{h}} = 27.86 \tag{3.9}$$

Hence,

$$v = \frac{2}{3t} \times \frac{\ln(p)}{(8 + \pi a/h)}) + \frac{(1/t - 1)}{(4 + 2.6a/h + 2.9h/a)} \tag{3.10}$$

Therefore,

$$q = u + v + uv = 0.162$$

$\varepsilon_{r.dyn}$ can be calculated using Eqs. (2.18)–(2.25) and (3.6)–(3.10) as

$$\varepsilon_{r.dyn}=1.94$$

and

$\varepsilon_{r,eff}$=2.12.

The fringing length ΔL may be computed as

$$\Delta L = \frac{\pi a\left[\sqrt{1+q} - 1\right]}{2\left[2.5 - 0.5\left(\frac{W}{L}\right)\right]} \tag{3.11}$$

=1.365.

Therefore, the resonant frequency $f_{r,10}$ becomes

$$f_{r,10} = \frac{c}{2\sqrt{\varepsilon_{r,eff}}}\frac{1}{L + 2\Delta L} = 4.916\,\text{GHz}$$

(b) Now, if h_2 = 1 mm,

$$\varepsilon_{re} = \frac{\varepsilon_r\left(1+\frac{h_1}{h_2}\right)}{(1+\varepsilon_r h_1/h_2)} = 1.56$$

$\varepsilon_{r.dyn} = 1.35$

and

$\varepsilon_{r.eff} = 1.43$

and

$$u = \left(1+\varepsilon_{re}^{-1}\right)\frac{4}{\frac{\pi a}{h}} = 0.278$$

$$t = 0.37 + 0.63\varepsilon_{re} = 1.337$$

$$p = \frac{1+0.8\left(\frac{a}{h}\right)^2+\left(\frac{0.31a}{h}\right)^4}{1+0.9\frac{a}{h}} = 9.83$$

Hence,

$$v = \frac{2}{3t}\times\frac{\ln(p)}{(8+\pi a/h)} + \frac{(1/t-1)}{(4+2.6a/h+2.9h/a)} = 0.0253$$

Therefore,

$$q = u + v + uv = 0.310$$

and hence

$$\Delta L = \frac{\pi a\left[\sqrt{1+q}-1\right]}{2\left[2.5-0.5\left(\frac{W}{L}\right)\right]} = 2.52$$

Therefore, the resonant frequency $f_{r.10}$ becomes

$$f_{r,10} = \frac{c}{2\sqrt{\varepsilon_{r,eff}}}\frac{1}{L+2\Delta L} = 5.37\,\text{GHz}$$

(a) Find out the input resonant resistance at the edge of a square patch with length 30 mm and width 30 mm, etched on a PTFE substrate of height 1.575 mm with dielectric constant 2.33.

(b)Find out the optimum feed position.

Solution:

(a) The input impedance of a patch can be expressed as

$$Z_{in}(f,x_0) = \frac{R_r}{1+Q_T^2\left(\bar{f}-\bar{f}^{-1}\right)^2} + j\left[X_f - \frac{R_r Q_T\left(\bar{f}-\bar{f}^{-1}\right)}{1+Q_T^2\left(\bar{f}-\bar{f}^{-1}\right)^2}\right] \tag{3.12}$$

http://dx.doi.org/10.5772/66355

where $\overline{f} = f/f_r$, f_r being the dominant mode resonant frequency and R_r is the input resistance at resonance at the edge of the patch.

Now, f_r can be obtained as done in the earlier example, and it is found to be f_r = 3.13 GHz.

R_r can be expressed as

$$R_r = \frac{4h}{\pi\lambda_0}\mu\eta_0 Q_T \left(\frac{L+2\Delta L}{W+2\Delta W}\right) cos^2\left(\frac{\pi(0.5L - x_0)}{L+2\Delta L}\right) \tag{3.13}$$

where η_0 = 377 Ω and x_0 is the distance from the centre of the patch and Q_T is the total quality factor, expressed in terms of the losses due to radiation (Q_r), dielectric (Q_d) and conductor (Q_c) present in the radiating structure as

$$Q_T = \left[\frac{1}{Q_r} + \frac{1}{Q_d} + \frac{1}{Q_c}\right]^{-1} \tag{3.14}$$

Now,

$$\lambda_0 = {}^{c}/_{f_r} = 95.84\text{mm} \tag{3.15}$$

ΔL can be obtained as done in the earlier example, and it is ΔL = 1.381 mm.

Now,

$$\Delta W = \Delta L\left(1.5 - \frac{W}{2L}\right) = 1.381\,\text{mm} \tag{3.16}$$

Now,

$$G_r = \frac{W^2}{90\lambda_0^2} \tag{3.17}$$

=0.001 as W = 30 mm which is smaller than 0.35 λ_0.

$$\varepsilon_{r,n} = \frac{\varepsilon_{reff} + 1}{2} = 1.165 \tag{3.18}$$

and

$$Z_r = \frac{120\pi\left[\frac{W}{h} + 1.393 + 0.667\ln\left(\frac{W}{h} + 1.444\right)\right]^{-1}}{\sqrt{\varepsilon_{r,n}}} \tag{3.19}$$

=13.41 Ω.

Q_r, Q_d, Q_c and Q_T can be calculated as

$$Q_r = \frac{\pi}{4G_r Z_r} = 53.76 \tag{3.20}$$

$$Q_d = \frac{\pi(\varepsilon_r - 1)\sqrt{\varepsilon_{r,n}}}{27.3(\varepsilon_{r,n} - 1)\sqrt{2\varepsilon_{r,n} - 1}} \frac{1}{tan\delta} = 232.19 \tag{3.21}$$

$$Q_c = h\sqrt{\pi f \mu_0 \sigma} = 1333.31 \tag{3.22}$$

$$Q_T = 42.27 \tag{3.23}$$

Therefore, the resonant resistance at edge (x_0 = 0.5 L)

$$R_r = \frac{4h}{\pi\lambda_0}\mu\eta_0 Q_T \left(\frac{L + 2\Delta L}{W + 2\Delta W}\right) cos^2\left(\frac{\pi(0.5L - x_0)}{L + 2\Delta L}\right) = 333.43\,\Omega.$$

(b) To obtain the optimum feed point, we need to find the point where input impedance of the patch becomes 50 Ω. From part (a), we get

L+ 2ΔL = 32.762 mm

W+ 2ΔW = 32.762 mm

Q_T = 42.27

R_r = 33.43 Ω

λ_g = 95.84 mm

Putting these in Eq. (3.3), we may write

$$\frac{4h}{\pi\lambda_0}\mu\eta_0 Q_T \left(\frac{L + 2\Delta L}{W + 2\Delta W}\right) cos^2\left(\frac{\pi(0.5L - x_0)}{L + 2\Delta L}\right) = 50 \tag{3.24}$$

or, (0.5L − x_0) = 12.23

or, x_0 = 2.77 mm.

4. Radiation characteristics

4.1. Gain enhancement

Any RMPA has a strong influence of substrate permittivity (ε_r) on its gain. In general, an RMPA experiences a decrease in gain with the increase of ε_r. Normally, an RMPA's gain is around 6 dBi when PTFE (ε_r = 2.33) is used as substrate. Here, we have discussed the role of air substrate on the gain enhancement issue of a simple RMPA. It is also found in an earlier work of one of the present authors in [41] that the use of air substrate leads to a symmetrical radiation pattern of an RMPA in its two principal planes.

The gain of an RMPA loaded with air substrate is directly related to its effective radiating area A_{eff}. Therefore, we can simply compare the change of the gain of an RMPA loaded with air substrate to a conventional (reference) RMPA loaded with PTFE (**Figure 5**) as discussed in an earlier work of one of the present authors in [41]:

$$\Delta G\, in\, dB = 10\log_{10}\left[\frac{\left(A_{eff}/\lambda_0^2\right)_{air}}{\left(A_{eff}/\lambda_0^2\right)_{ref}}\right] \tag{4.1}$$

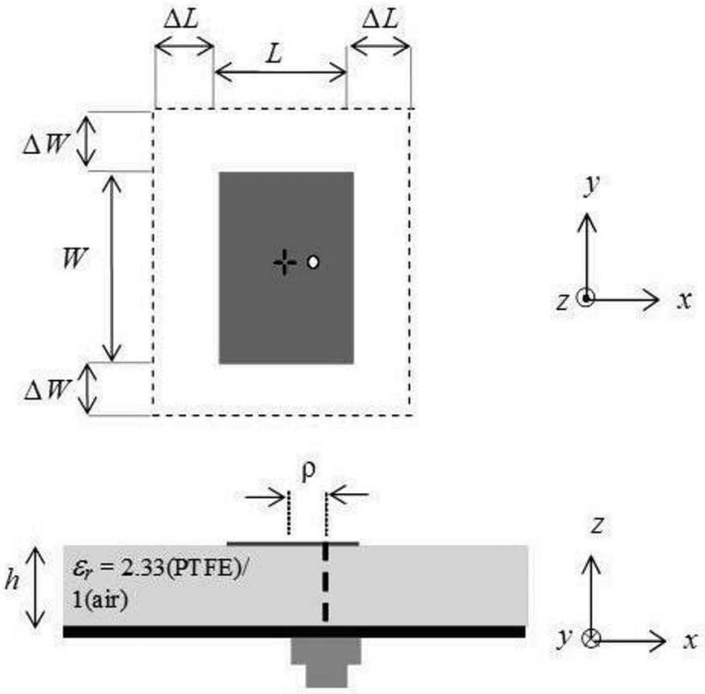

Figure 5. Schematic diagram of a rectangular patch using conventional PTFE (ε_r = 2.33) or air substrate (ε_r = 1): top and cross-sectional views.

where λ_0 is the operating wavelength. For a rectangular patch, as shown in **Figure 5**, its effective radiating area (A_{eff}) may be calculated as given in an earlier work of one of the present authors in [41]:

$$A_{eff} = (L + 2\Delta L)(W + 2\Delta W) \tag{4.2}$$

where L and W are the physical length and width of the corresponding patch, respectively. The quantities ΔL and ΔW represent the effective increments in respective dimensions caused by the fringing electric fields (discussed in Section 2.1).

Now, the standard formula of gain (G) of any rectangular aperture is (as given in one of the earlier works of the authors in [42])

$$G = \frac{4\pi A_{eff}}{\lambda^2} = \varepsilon_{ap}\frac{4\pi A_p}{\lambda^2} \tag{4.3}$$

where A_p is the physical aperture, respectively, and ε_{ap} is the aperture efficiency. Following Eq. (4.3) we can write the expression for gain of an RMPA from our earlier work in [42]

$$G = \frac{4\pi(L + 2\Delta L)(W + 2\Delta W)}{\lambda^2} \tag{4.4}$$

It is seen that when air substrate is used in lieu of PTFE substrate, the electric field lines along the patch edges becomes more relaxed or loosely bound resulting in an increase in ΔL and ΔW, and hence A_{eff} increases. Therefore, gain increases.

The formulations presented in this section are well validated against simulations and measurements [36, 41]. These formulations are found to be very much accurate for L-Ku band and for wide range of aspect ratios. **Figure 6** shows increase in gain when PTFE substrate is replaced by air substrate for *W*/*L* ratio 1.5.

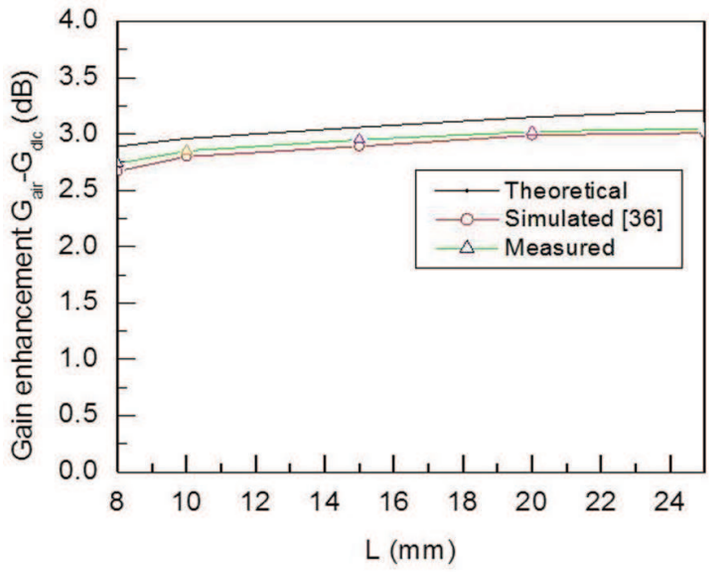

Figure 6. Variation of the gain enhancement between the microstrip patches with air and PTFE substrate for different sets of patches having the most common aspect ratio (*W*/*L* = 1.5) for ε_r = 2.33.

Theoretically computed, simulated and measurement results show very close agreement among themselves.

4.2. Polarization purity

In general, a conventional RMPA radiates in the fundamental TM_{10} mode along the broadside of the element, and the field is primarily linearly polarized, called co-polarized (CO) radiation. However, some orthogonally polarized, called cross polarized (XP), radiations take place due to weak oscillations of higher-order modes inside an RMPA. The XP radiation becomes considerably prominent for probe-fed designs particularly when the thicknesses as well as the dielectric constant of the substrate increase. Thus, the XP radiation becomes an important issue for investigation for microstrip antenna research. The (XP) fields are more significant in H plane than in E plane as obtained in our earlier work in [45]. Therefore, the polarization purity (CO-XP isolation) deteriorates in H plane (only 9 dB), and the suppression of XP radiation performance of an RMPA to improve its polarization purity is the challenging issue for antenna research community. Lower polarization purity also limits the use of RMPA in different array applications There are several techniques to improve polarization purity of an RMPA such as the use of defected ground structure (DGS) [11], grounding the non-radiating

http://dx.doi.org/10.5772/66355

edges of a patch [43, 45] and defected patch surface [46]. A thorough discussion on DGS-integrated RMPAs can be found in [11, 42]. However, DGS-integrated RMPAs always possess high back radiation, and only 15–20 dB of CO-XP isolation in H plane can be obtained from those [11, 42]. The two later techniques can address the limitations of DGS and minimum 25 dB of CO-XP isolation from those, and these are discussed clearly in this section. The two techniques are very simple to understand and very effective to implement over a wide microwave frequency range (L-Ku band).

An RMPA with three pairs of shorting plates placed at the non-radiating edges is shown in **Figure 7**. If the non-radiating edges are grounded using pairs of thin strips, the EM boundary conditions get altered and result in a significant change in field structure with in the cavity. Hence, the restructuring of field structure within the patch inevitably modifies the radiation properties of the RMPA. Some recent work in [43, 44] show the XP radiations are typically from the non-radiating edges of the RMPA. In fact, the oscillations of electric field beneath the patch in a direction, orthogonal to E plane, produce higher-order orthogonal resonance (higher-order orthogonal modes). The XP radiations are typically due to those higher-order orthogonal modes and the fields of those modes, located near the non-radiating edges of the patch. The electric field vectors for a grounded patch in TM_{np} mode may be obtained from our earlier work in [45] as

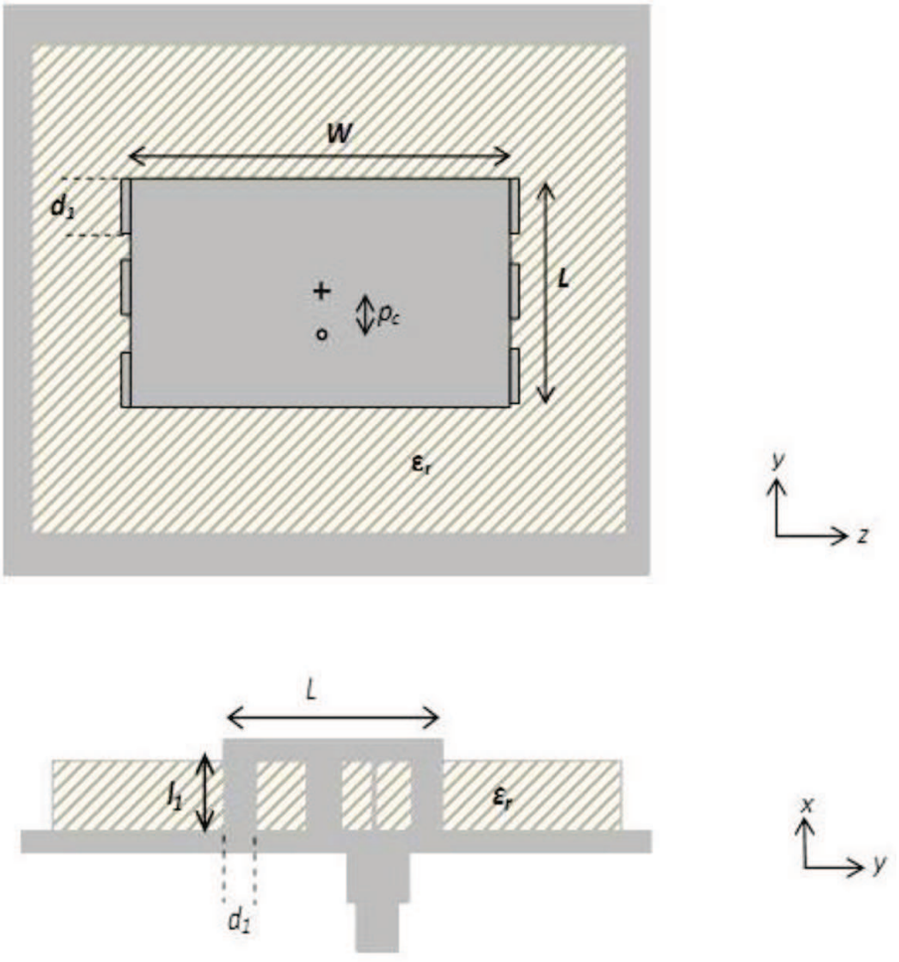

Figure 7. Schematic diagram of an RMPA with shorting strips. (a) Top view and (b) side view (L and W are the length and width of the patch, l_1 and d_1 are length and width of the shorting plates, ε_r is the dielectric constant of the substrate and p_c is the feed position).

$$E_x \propto \cos\left(\frac{n\pi}{L}y'\right)\sin\left(\frac{p\pi}{W}z'\right) \tag{4.5a}$$

$$H_y \propto \cos\left(\frac{n\pi}{L}y'\right)\cos\left(\frac{p\pi}{W}z'\right) \tag{4.5b}$$

$$H_z \propto \cos\left(\frac{n\pi}{L}y'\right)\sin\left(\frac{p\pi}{W}z'\right) \tag{4.5c}$$

where E_x, H_y and H_z are the electric and magnetic field components of the dominant mode. The number of half-wave variations along the length and width of the patch is denoted by n and p, respectively.

The electric surface current over the patch surface can be obtained from our earlier work in [45] as

$$J_s = \hat{n} \times H \tag{4.6}$$

The co-sinusoidal variation in Eq. (4.5) shows the variation of E_x along the length (L) of the patch, while the sinusoidal variation shows the variation of E_x along the orthogonal direction. Therefore, any higher-order orthogonal resonance (i.e. for any non-zero value of p) leads to minimum electric field intensity when z approaches W. In fact, the intensity of the electric fields near the non-radiating edges due to all higher-order orthogonal modes (primarily responsible for XP radiation) is forced to be minimum in order to mitigate the possibility of XP radiation from non-radiating edges due to higher-order orthogonal modes [45]. It is also seen that when the non-radiating edges are grounded with thin metallic strips, the electric fields near the non-radiating edges have least intensity when compared with the electric field intensity at the central region, but the dominant mode radiation characteristics remain unaltered. From the literature it is seen that the XP radiation from RMPA is typically from the non-radiating edges, and those are due to asymmetric field distribution along the length of the patch [43, 45]. This asymmetry in the field distribution is mainly due to the placement of feeding probe and is unavoidable for probe-fed patch. This asymmetry in the field causes asymmetry in the electric surface current (J_s) along the patch length (as discussed in our previous work in [45]). For a conventional RMPA, the y component of J_s does not become maximum at the centre [45]. This y component of J_s attributes for high XP radiation from RMPA. However, in our earlier work in [45], the use of grounded strips in case of an RMPA shows a change of the field structure beneath the patch as a result of which the electric surface current at non-radiating edge does not follow the conventional profile. Therefore, XP radiations are mitigated keeping CO radiation unaltered.

The use of grounded strip loading in a conventional RMPA not only modifies the radiation property but also regulates the input characteristics of the RMPA [45]. The length (l_1) of each thin grounding strip is essentially same as substrate thickness h, and when it is in the order of $\lambda/10$, one can write as discussed in our previous work in [45]:

$$l_1 = \lambda_{gr}/10 \tag{4.7}$$

$$\lambda_{gr} = \lambda_r/\sqrt{\varepsilon_r} \tag{4.8}$$

http://dx.doi.org/10.5772/66355

$$\lambda_r = c/f_r \tag{4.9}$$

where f_r is dominant mode resonant frequency, λ_{gr} is the resonant wavelength within dielectric and ε_r is the dielectric constant of substrate material.

The width of the strips (d_1) is considered to be very thin. Each grounded strip or short dipole ($l_1 \times d_1$) produces the reactive impedance [45, 47] as

$$X_s = 30\left\{2Si(kl_1) + \cos(kl_1)[2Si(kl_1) - Si(2kl_1)] - sin(kl_1)\left[2Ci(kl_1) - Ci(2kl_1) - Ci\left(\frac{2kd_1'^2}{l_1}\right)\right]\right\} \tag{4.10}$$

which comes parallel to patch input impedance (Z_p). Here, $d_1'^2$ is the equivalent circular radius of dipole of width d_1. For the dipole of noncircular cross section, $d_1'^2$ (as discussed in our previous work in [45])

$$d_1'^2 = 0.25d_1 \tag{4.11}$$

Therefore, from [45]

$$kl_1 = \frac{2\pi}{\lambda_g}\frac{\lambda_{gr}}{10} = 0.628\frac{f}{f_r} \tag{4.12}$$

and

$$\frac{2kd_1'^2}{l_1} = \frac{7.85ff_rd_1^2\varepsilon_r}{c^2} \tag{4.13}$$

The expression for reactive impedance can be written as [45]

$$X_s = 30\left\{2Si\left(0.628\frac{f}{f_r}\right) + \cos\left(0.628\frac{f}{f_r}\right)\left[2Si\left(0.628\frac{f}{f_r}\right) - Si\left(2\times0.628\frac{f}{f_r}\right)\right]\right.$$
$$\left. - \sin\left(0.628\frac{f}{f_r}\right)\left[2Ci\left(0.628\frac{f}{f_r}\right) - Ci\left(2\times0.628\frac{f}{f_r}\right) - Ci\left(\frac{7.85ff_rd_1^2\varepsilon_r}{c^2}\right)\right]\right\}. \tag{4.14}$$

The input impedance of conventional probe-fed RMPA can be written as

$$Z_p = \frac{1}{\left(1/R_r\right) + j\omega C + \left(1/j\omega L\right)} \tag{4.15}$$

where R_r is the resonant resistance of the patch at particular feed position. C and L are capacitance and inductance, respectively, and can be obtained from [9]. When this conventional probe-fed RMPA is loaded with short dipoles, the dipole reactance (X_s) will come in parallel to patch, and the resultant input impedance of dipole loaded patch can be written as [45, 47]

$$Z_{dp} = \frac{1}{\left(1/R_r\right) + j\omega C + \left(1/j\omega L\right) + jX_s} \tag{4.16}$$

Putting the values of C and L from [9]

$$Z_{dp} = \frac{1}{\left(1/R_r\right) + j\left[\frac{fQ_T}{f_r R_r} - \frac{f_r Q_T}{fR_r} + jX_s\right]} \tag{4.17}$$

where Q_T is the total quality factor.

Hence,

$$Re\left(Z_{dp}\right) = \frac{1/R_r}{\left(1/R_r\right)2 + j\left[\frac{fQ_T}{f_r R_r} - \frac{f_r Q_T}{fR_r} + jX_s\right]^2} \tag{4.18}$$

$$Im\left(Z_{dp}\right) = X_f - \frac{\left[\frac{fQ_T}{f_r R_r} - \frac{f_r Q_T}{fR_r} + jX_s\right]}{\left(1/R_r\right)^2 + j\left[\frac{fQ_T}{f_r R_r} - \frac{f_r Q_T}{fR_r} + jX_s\right]^2} \tag{4.19}$$

where X_f is the feed reactance and can be obtained from [36].

From our earlier work in [45], it is observed that when grounded strips are placed along the non-radiating edges, the structure becomes thick dipole loaded (dipole length to diameter ratio ~ 4.2 around resonant frequency), and it prevents the usual sharp variation of input reactance over the operating bandwidth. It is found from our previous work in [45] that the reactance of thick dipole slowly varies with the frequency, and as it is in parallel to patch reactance, the resultant reactance of the proposed patch varies slowly with frequency (**Figure 8**).

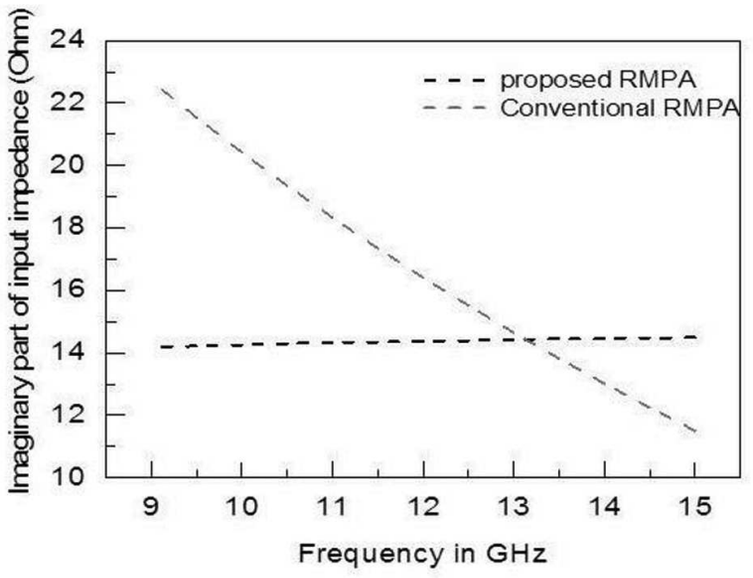

Figure 8. Variations of imaginary part of input impedance (input reactance) as a function of frequency for conventional and proposed RMPA. (Total quality factor Q_T = 0.22, resonant resistance R_r = 50 Ω and L = 8 mm, W = 12 mm, h = 1.575 mm, ε_r = 2.33, feed reactance X_f = 15 Ω). Reproduced with permission of © 2016 FREQUENZ [45].

The formulations presented in this section were validated in case of an RMPA with length L = 8 mm and W = 12 mm designed over Taconic's TLY-3-0620 PTFE material (ε_r = 2.33) with thickness h = 1.575 mm [45]. The ground plane dimensions were taken as 80 × 80 mm^2.

Three pairs of thin copper strips of thickness 0.1 mm with height of $h = l_1$ = 1.575 mm and width d_1 = 1.5 mm have been placed along the non-radiating edges (**Figure 7**). Around 25–40 dB of minimum CO-XP isolation in H plane along with input impedance of 1.32 GHz is found from the patch (see **Figure 9**) [45].

In E plane, CO-XP isolation is more than 35 dB (**Figure 10**).

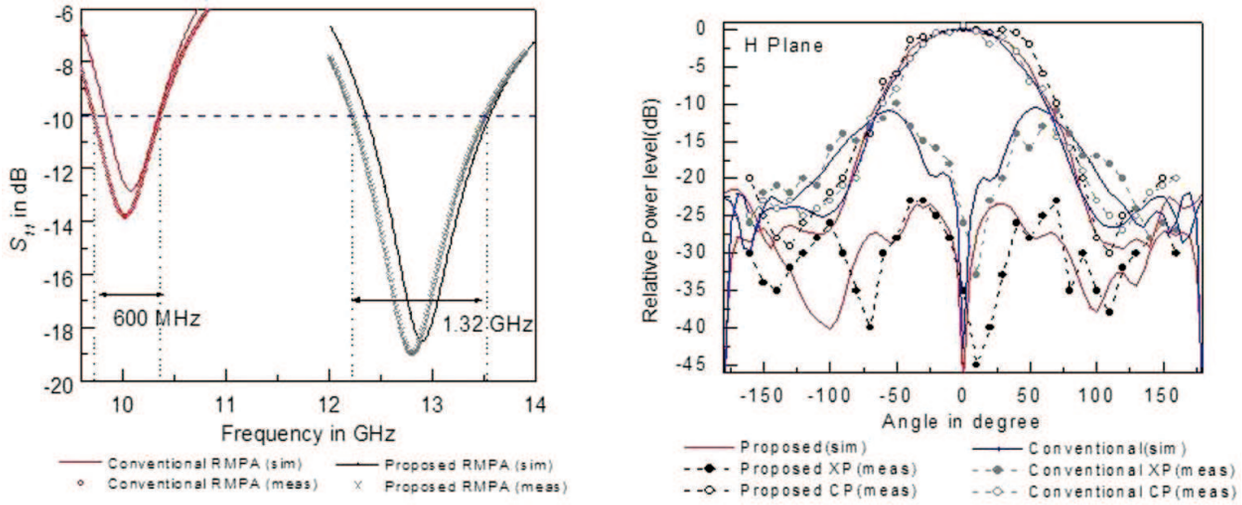

Figure 9. Simulation and measured reflection coefficient profile for conventional and proposed RMPA and simulated and measured radiation patterns for conventional (f = 10.05 GHz) and proposed RMPA (f = 12.9 GHz) at fundamental resonant mode in H plane. Reproduced with permission of © 2016 FREQUENZ [45].

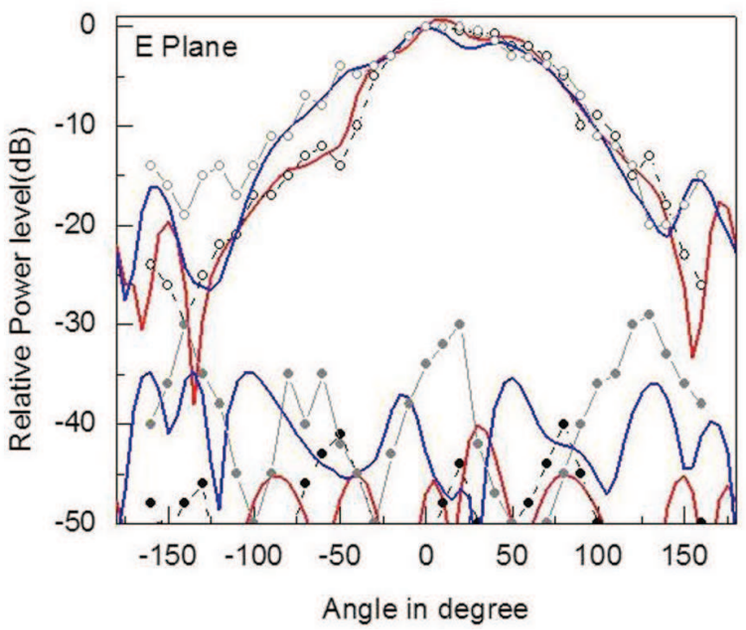

Figure 10. Comparison of simulated and measured radiation patterns for conventional (f = 10.05 GHz) and proposed RMPA (f = 12.9 GHz) at fundamental resonant mode in E plane. Reproduced with permission of © 2016 FREQUENZ [45].

One can write the field components corresponding to TM_{02} mode beneath the patch as discussed in our previous work in] (see **Figure 11** for coordinates) [46]:

$$E_x = C\cos\left(\frac{2\pi}{W}z\right) \tag{4.20}$$

$$H_y = C\sin\left(\frac{2\pi}{W}z\right) \tag{4.21}$$

Eqs. (4.20 and 4.21) show that at z = 0 and at $z = W/2$, E_x is maximum and is equal to C.

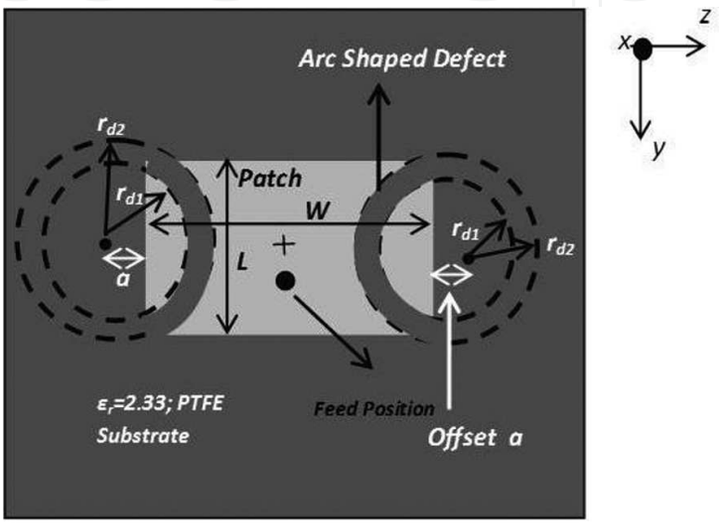

Figure 11. Schematic diagram of an RMPA with arc-defected patch surface (*top view*).

Hence, the null occurs in between these limits, i.e. [46]

$$E_x = C\cos\left(\frac{2\pi}{W}z\right) = 0 \text{ for } 0 < z < W/2 \tag{4.22}$$

From Eq. (4.22) one can write that

$$\frac{2\pi}{W}z_1 = \frac{m\pi}{2} \text{ where } \mathrm{m} = 1, 3, 5, \ldots \tag{4.23}$$

Therefore,

$$z_1 = \frac{mW}{4} = \frac{W}{4} \tag{4.24}$$

Along the middle section of the patch, i.e. when $W \to 0$; , 97% of the maximum field exists (as discussed in our earlier work in [46]) if

$$E_x = C\cos\left(\frac{2\pi}{W}z\right) = 0.97C \tag{4.25}$$

Hence, from our previous work in [46], we can write

$$\frac{2\pi}{W}z_2 = \cos^{-1}(0.97) = \frac{2\pi}{25} \tag{4.26}$$

Therefore,

$$z_2 = \frac{W}{25} \tag{4.27}$$

A defect can be incorporated within this region, i.e. from z_1 to z_2. This in fact will perturb the fields corresponding to TM_{02} mode which is mainly responsible for XP radiation.

The electric surface current (J_s) on the patch surface corresponding to TM_{02} mode can be written as given in our earlier work in [46]:

$$J_s = \hat{n} \times H = \hat{a_x} \times |H_y| \hat{a_y} \tag{4.28}$$

Therefore,

$$J_s = \left| C sin \frac{2\pi}{W} z \right| \hat{a_z} \tag{4.29}$$

In case of an RMPA with length $L = 8$ mm and width $W = 12$ mm, the value of z_1 and z_2 is found to be 3 mm and 0.5 mm [46]. Based on the formulations described here, an arc-shaped defect has been cut on patch ($L = 8$ mm and $W = 12$ mm) symmetrically along the non-radiating edges as shown in **Figure 11** in our earlier work in [46]. The centre of the arc defect (a) is chosen in such a way that the defect can be cut through the patch corners. Around 25–35 dB, CO-XP isolation is reported from such an RMPA in H plane with such arc-shaped defect over the patch surface in [46]. However, the bandwidth is comparable with that of a conventional RMPA. Therefore, it can be observed that the effect of TM_{02} mode can be mitigated to a large extent by opting either grounding the non-radiating edges of an RMPA or judicious incorporation of defects over the patch surface. Such types of new antenna structures are surely be utmost useful for scientific and research community for designing low-profile wireless communication devices where polarization purity is required to establish over the whole operating band.

5. Conclusion

In this chapter, some recent developments in the CAD techniques have been presented lucidly but thoroughly for rectangular microstrip antennas. The presented formulations are very much accurate and are valid for wide range of aspect ratios and substrate thickness compared to other formulations. It is hoped that the work would be helpful for researchers and engineers working in the field of microstrip antennas and will help them to gain an insight into the physics of any RMPA.

Acknowledgements

Authors would like to express their deep sense of gratitude to Prof. L. Lolit Kumar Singh of Mizoram University, Mizoram; Prof. Gautam Das of Siliguri Institute of Technology, West Bengal; Prof. Debatosh Guha and Dr. Jawad Y. Siddiqui of the Institute of Radio Physics and Electronics, Calcutta University and Prof. B. N. Basu of Sir. J. C. Bose School of Engineering, Mankundu, West Bengal, India, for fruitful discussions during the preparation of the manuscript.

Subhradeep Chakraborty thanks Prof. Santanu Chaudhury, Director, CSIR-CEERI, Pilani; Dr. S. N. Joshi, Ex-Emeritus Scientist; Chirag P. Mistry, Scientist, TWT Group; Dr. Amitavo Roy Choudhury, Senior Scientist, TWT Group; Dr. Sanjay Kumar Ghosh, Principal Scientist and Head of TWT Group and Dr. R. K. Sharma, Principal Scientist and Head of MWT Division, CSIR-CEERI, Pilani, for always encouraging research endeavours and their support.

Author details

Sudipta Chattopadhyay[1]* and Subhradeep Chakraborty[2]

*Address all correspondence to: sudipta_tutun@yahoo.co.in

1 Department of Electronics and Communication Engineering, Mizoram University, Aizawl, Mizoram, India

2 TWT Group, MWT Division, CSIR-Central Electronics Engineering Research Institute, Pilani, Rajasthan, India

References

[1] Deschamp G., Sichak W., Microstrip microwave antennas. In: Third symposium on the USAF antenna research and development program; October 18, 1953; October 22, 1953. USA:1953.

[2] Howell J.Q., Microstrip antennas. IEEE Trans. Antennas Propag. 1972;**23**:90–93. DOI: 10.1109/TAP.1975.1141009.

[3] Munson R.E., Conformal microstrip antennas and microstrip phased arrays. IEEE Trans. Antennas Propag., 1974;**25**:74–78. DOI: 10.1109/TAP.1974.1140723.

[4] Bahl I.J., Bhartia P., Microstrip Antennas. USA: Artech House; 1980.

[5] Lee K.F., Luk K.M., Microstrip Patch Antennas. UK: Imperial College Press; 2011.

[6] James J.R., Hall P.S., Wood C., Microstrip Antennas: Theory and Design. London: Peter Peregrinus; 1981.

[7] James J.R., Hall P.S., editors. Handbook of Microstrip Antennas. London: Peter Peregrinus; 1989.

[8] Lee K.F., Chen W., editors. Advances in Microstrip and Printed Antennas. New York: JohnWiley& Sons Ltd; 1997.

[9] Garg R., Bhal I., Bhartia P., Ittpiboon A., Microstrip Antenna Design Handbook. Boston, USA: Artech House; 2001.

[10] Volakis J., editors. Antenna Engineering Handbook. New York: McGraw-Hill; 2007.

[11] Guha D., Antar Y.M.M., editors. Microstrip and Printed Antennas: New Trends, Techniques and Applications. UK: Wiley; 2011.

[12] Pozar D.M., Schaubert D.H., editors. Microstrip Antennas, IEEE Press, New York:1995.

[13] Gupta K.C., Benella A., editors. Microstrip Antenna Design. USA: Artech House; 1988.

[14] Chattopadhyay S., Biswas M., Siddiqui J.Y., Guha D., Rectangular microstrips with variable air gap and varying aspect ratio: improved formulations and experiments. Microw. Opt. Technol. Lett. 2009;**51**:169–173. DOI: 10.1002/mop.24025.

[15] Hammerstad E.O., Equations for Microstrip Circuit Design. In: 5th European Microwav. Conf; Hamburg:1975. pp. 268–272.

[16] Garg R., Long S.A., Resonant frequency of electrically thick rectangular microstrip antennas. Electron. Lett. 1987;**23**:1149–1151. DOI: 10.1049/el:19870801.

[17] Abboud F., Damiano J.P., Papiernik A., Simple model for the input impedance of coax-fed rectangular microstrip patch antenna for CAD. IEE Proc. Microw. Antennas Propag. 1988;**135**:323–326. DOI: 10.1049/ip-h-2.1988.0066.

[18] Thouroude D., Himdi M., Daniel J.P., CAD oriented cavity model for rectangular patches. Electron. Lett. 1990;**26**:842–844. DOI: 10.1049/el:19900552.

[19] Pues H., Vande Capelle A., Accurate transmission line model for the rectangular microstrip antenna. IEE Proc. 1984:334–340. DOI: 10.1049/ip-h-1.1984.0071.

[20] Bhattacharya A.K., Long rectangular patch antenna with a single feed. IEEE Trans. Antennas Propag. 1990;**38**:987–993. DOI: 10.1109/8.55609.

[21] Newman E.H., Tulyathan P., Analysis of microstrip antennas using moment methods. IEEE Trans. Antennas Propag. 1981;**29**:47–53. DOI: 10.1109/TAP.1981.1142532.

[22] Ridgers G.M., Odendaal J.W., Joubert J., Entire-domain versus subdomain attachment modes for the spectral-domain method of moments analysis of probe-fed microstrip patch antennas. IEEE Trans. Antennas Propag. 2004;**52**:1616–1620. DOI: 10.1109/TAP.2004.829401.

[23] Chew W.C., Liu Q., Resonance frequency of a rectangular microstrip patch. IEEE Trans. Antennas Propag. 1988;**36**:1045–1056. DOI: 10.1109/8.7216.

[24] Chang E., Long S.A., Richards W.F., Experimental investigation of Electrically thick rectangular microstrip antennas. IEEE Trans. Antennas Propag. 1986;**34**:767–772. DOI: 10.1109/TAP.1986.1143890.

[25] Kara M., Design consideration for rectangular microstrip antenna elements with various substrate thickness. Microw. Opt. Technol. Lett. 1998;**19**:111–121. DOI: 10.1002/(SICI) 1098-2760(19981005).

[26] Lee K.F., Ho K.Y., Dahele J.S., Circular disc microstrip antenna with an air-gap. IEEE Trans. on Antennas Propag. 1984;**32**:880–884. DOI: 10.1109/TAP.1984.1143428.

[27] Guha D., Resonant frequency of circular microstrip antennas with and without air-gaps. IEEE Trans. Antennas Propag. 2001;**49**:55–59. DOI: 10.1109/8.910530.

[28] Abboud F., Damino J.P., Papiernik A., Accurate Model for The Input Impedance of Coax-Fed Rctangular Microstrip Antenna With and Without Air-Gaps. In: International Conference on Antennas and Propagation; 1989. pp. 102–106.

[29] Fan Z., Lee K.F., Spectral domain analysis of rectangular microstrip antennas with an air-gap. Microw. Opt.Technol. Lett. 1992; **5**:315–318. DOI: 10.1002/mop.4650050708.

[30] Qiu J., Huang Y., Wang A., An Improved Model for the Resonant Frequency of Tunable Rectangular Microstrip Antenna. In: International Conference on Microwave and Milimeter Wave Technology; 2002. pp. 524–527.

[31] Fortaki T., Khedrouche D., Bouttout F., Benghalia A., A numerically efficient full-wave analysis of a tunable rectangular microstrip patch. Int. J. Electron. 2004;**91**:57–70. DOI: 10.1080/00207210310001656097.

[32] Zhong S.S., Liu G., Quasim G., Closed form expression for resonant frequency of rectangular patch antennas with multi dielectric layers. IEEE Trans. Antennas Propag. 1994;**42**:1360–1363. DOI: 10.1109/8.318667.

[33] Schaubert D., Pozar D., Adrian A., Effect of microstrip antenna substrate thickness and permittivity: comparison of theories and experiment. IEEE Trans. Antennas Propag. 1989;**37**:677–682. DOI: 10.1109/8.29353.

[34] Gauthier G.P., Courtay A., Rebeiz G.M., Microstrip antennas on synthesized low dielectric constant substrates. IEEE Trans. Antennas Propag. 1997;**45**:1310–1314. DOI: 10.1109/8.611252.

[35] Chattopadhyay S., Theoretical and Experimental Studies of Some Aspects of a Rectangular Microstrip Patch Antenna [Thesis]. Kolkata: University of Calcutta; 2011.

[36] HFSS: High Frequency Structure Simulator, Ansoft Corp.version 11, USA.

[37] Guha D., Siddiqui J.Y., Resonant frequency of circular microstrip antenna covered with dielectric superstrate. IEEE Trans. Antennas Propag. 2003;**51**:1649–1652. DOI: 10.1109/TAP.2003.813620.

[38] Wolff I., Knoppik N., Rectangular and circular microstrip disk capacitors and resonators. IEEE Trans. Microw. Theory Tech. 1974;**22**:857–864. DOI: 10.1109/TMTT.1974.1128364.

[39] Guha D., Antar Y.M.M., Siddiqui J.Y., Biswas M., Resonant resistance of probe and microstrip line-fed circular microstrip patches. IEE Proc. Microw. Antennas Propag. 2005;**152**:481–484. DOI: 10.1049/ip-map:20045161.

[40] Chattopadhyay S., Biswas M., Siddiqui J.Y., Guha D. Input impedance of probe fed rectangular microstrip antenna with air gap and aspect ratio. IET Microw. Antennas Propag. 2009;**3**:1151–1156. DOI: 10.1049/iet-map.2008.0320.

[41] Guha D., Chattopadhyay S., Siddiqui J.Y., Estimation of gain enhancement replacing PTFE by air substrate in a microstrip patch antenna. IEEE Antennas. Propag. Mag. 2010;**52**:92–95. DOI: 10.1109/MAP.2010.5586581.

[42] Chakraborty S., Chattopadhyay S., Substrate fields modulation with defected ground structure: a key to realize high gain, wideband microstrip antenna with improved polarization purity in principal and diagonal planes. Int. J. RF and Microw. Computer Aided Eng. (RFMiCAE), Wiley, USA. 2016;**26**:174–181. DOI: 10.1002/mmce.

[43] Ghosh D., Ghosh S.K., Chattopadhyay S., Nandi S., Chakraborty D., Anand R., Raj R., Ghosh A., Physical and quantitative analysis of compact rectangular microstrip antenna with shorted non-radiating edges for reduced cross-polarized radiation using modified cavity model. IEEE Antennas Propag. Mag. 2014;**56**:61–72. DOI: 10.1109/LAWP.2014.2363563.

[44] Ghosh A., Ghosh D., Chattopadhyay S., Singh L.L.K., Rectangular microstrip antenna on slot type defected ground for reduced cross polarized radiation. IEEE Antennas Wirel. Propag. Lett. 2014;**14**:321–324. DOI: 10.1109/LAWP.2014.2363563.

[45] Poddar R.P., Chakraborty S., Chattopadhyay S., Improved cross polarization and broad impedance bandwidth from simple single element shorted rectangular microstrip patch: theory and experiment. FREQUENZ. 2016;DOI: 10.1515/freq-2015-0105.

[46] Shivnarayan S.S., Vishvakarma B.R., Analysis of slot loaded rectangular microstrip patch antenna, Indian J. Radio Space Phys., 2005; **34**:424–430.

[47] Balanis, C.A., Antenna Theory: Analysis and Design. 2nd ed. Wiley; USA, 2001.

IntechOpen